PHYSICAL REVIEW E **73**, 065304(R) (2006)

Effective front propagation in steady cellular flows: A least time criterion

A. Pocheau and F. Harambat
IRPHE, CNRS et Universités Aix-Marseille I & II, 49 rue Joliot-Curie, B.P. 146, Technopôle de Château-Gombert, F-13384 Marseille, Cedex 13, France

(Received 7 December 2005; published 20 June 2006)

We experimentally study the propagation of a reaction front in a chain of counter-rotating vortices. The front is induced by an autocatalytic chemical reaction in an aqueous solution stirred by electroconvective means. The front propagates by getting quickly engulfed in a vortex and by slowly crossing the separatrix to the next vortex. Its mean velocity along the chain increases with the flow intensity but shows both a bending and a dependence on the vortex aspect ratio. We recover these features within a kinematic model of front propagation by seeking the quickest front path through a vortex.

DOI: 10.1103/PhysRevE.73.065304 PACS number(s): 47.70.Fw, 45.10.Db, 47.15.−x

Propagation of a front in a stirred medium stands as an essential transport process in many fields of science and technology including chemical systems [1], combustion [2], or population dynamics [3]. Its net efficiency results from a competition between a nonlinear reaction-diffusion process that seeks to maintain sharp gradients and a stirring advection process that aims at a large scale homogenization. In particular, in many usual regimes, stirring induces front wrinkles that increase the reaction surface in the medium and, finally, the effective reaction rate. This mechanism is especially efficient in multiscale flows where the enhancement of front velocity by turbulence can even reach an order of magnitude [2]. It has motivated extensive statistical analysis to determine the cumulative effects of the flow scales. However, the basic phenomenon of velocity enhancement at a single scale has comparatively received little attention, especially on the experimental ground. Yet, it is more appropriate to analyze the mechanism of front propagation in an advective medium and to identify the relevant ways for modeling it in more complex situations.

Previous experiments on single scale flows have been performed either in gaseous combustion [4] or in aqueous solutions [5,6]. The former was not suited to easily control flows because of the gas expansion induced by extensive heat release. The latter involve autocatalytic reactions that negligibly perturb flows. They have been used in Poiseuille flows [5] and in oscillating cellular flows [6]. Here, we use them to investigate the mechanism of front propagation in a *steady cellular* vortex flow [7]. Two-dimensional numerical simulations of this issue have led to models based on renormalization [8] and on a one-dimensional kinematics of the front head [9]. The former provides a universal scaling law for the enhancement of front velocity by stirring, and the latter calls for a numerical determination of an integral parameter on the unknown trajectories. In contrast, we shall find here that the effective front velocity also depends on the third dimension, the vortex depth, and that the actual front trajectory can be determined as the quickest trajectory among a suitable family. This selection principle, reminiscent of Fermat's least time principle, will allow us to recover the actual effective front velocity and its dependence on the vortex aspect ratio.

The experiment is performed in a 200-mm-long, narrow, and thin channel filled with sodium chlorite and potassium iodide solutions at suitable concentrations for providing an autocatalytic reaction between chlorite and iodide [10] (Fig. 1). Front visualization is achieved by adding a starch indicator which colors the initial medium but which disappears as the front passes through. The front is then localized at the frontier between the colored and the colorless media (Fig. 2). A cellular flow is generated in the ionic solution by electroconvection (Fig. 1) [11]. A series of magnets, 20-mm long, are placed below the channel so that their magnetic field crosses the fluid layer in alternate directions. An electric current then produces Laplace forces that induce a series of ten counter-rotating vortices centered on each magnet.

The concentration of chlorite and iodide is set to 3.0 and 3.75×10^{-4} mol/l and a buffer solution stabilizes the pH at 5. This yields a front thickness $\lambda\approx1$ mm, a reaction time $\tau_r\approx6$ s, a diffusivity of species $D\approx2\times10^{-9}$ m^2 s^{-1}, and an intrinsic front velocity $V_o\approx2$ mm/mn. The electric current was kept below 3 mA. It slightly increases the front velocity when directed in the direction of propagation, $dV_o/dI=0.26$ mm mn^{-1} A^{-1}, and negligibly in the opposite direction, $dV_o/dI=0.03$ mm mn^{-1} A^{-1}. The major experimental uncertainty comes from the flow velocity and amounts to 10% in relative value.

Two channel widths, $l=6$ and 12 mm, have been used with a single depth $d=3$ mm. Care has been taken to restrict the flow intensity U so as to remain in the Hele–Shaw regime where the top and bottom boundary layers overlap: $U<20$ mm/mn for $d=6$ mm and $U<40$ mm/mn for $d=12$ mm. In this hydrodynamical regime, the boundary layer thickness amounts to half the cell depth $d/2$ on *all* boundaries including the channel sides that bound vortices (Fig. 1).

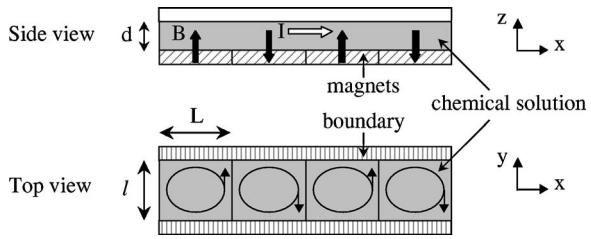

FIG. 1. Sketch of the experimental setup showing the fluid channel with its top and lateral boundaries, the magnets, the magnetic field B, the electric current I, and the resulting electroconvective vortices. The actual dimensions are $L=20$ mm, $l=6$ or 12 mm, and $d=3$ mm.

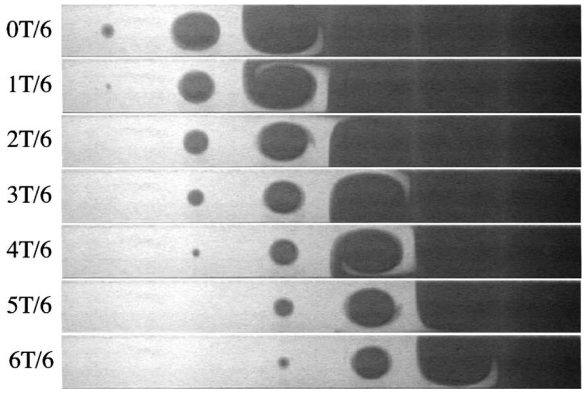

FIG. 2. Top view of a front propagating from left to right at proper velocity $V_o=1.6$ mm mn^{-1}, reduced flow intensity $U/V_o=18.8$, and reduced effective velocity $V_f/V_o=7.8$. Vortex length, width, and depth are 20, 12, and 3 mm. During the time period $T=192$ s, the front advances over a pair of counter-rotating vortices, on a distance $2L=40$ mm. Whereas it is quickly advected in a vortex, its velocity is only V_o toward the vortex centers and at the crossing of separatrix.

Implications of a narrow dimension d on front propagation depend on the ratio $\eta=dV_o/2D$ [5,12]. Its large value, 25 here, places the experiment in the large gap limit where the local front velocity V is set by the component of the flow velocity on the direction of propagation $\mathbf{n}$. In particular, for a front comoving with the flow, $\mathbf{U}\cdot\mathbf{n}>0$, the front profile in the channel depth is such that $V=V_o+\mathbf{U}\cdot\mathbf{n}$ where U denotes the maximum flow velocity in the gap and where curvature effects are neglected. This means that the front advances at its proper velocity V_o with respect to the advective medium and thus satisfies an eïkonal dynamics.

In the present closed cellular flow, the relative importance of advection, diffusion, and reaction is set by nondimensional numbers based on the vortex scale L: the Péclet number $\mathrm{Pe}=UL/D$, the Damköhler number $\mathrm{Da}=L/U\tau_r$, and the scale ratio $\xi=L/\lambda$ between vortex size and front thickness. The experiment stands in the large Péclet, large Damköhler, and large vortex regime, $\mathrm{Pe}>250$, $\mathrm{Da}>5.8$, $\xi=20$, where the front structure remains locally unchanged despite stirring, in agreement with an eïkonal dynamics.

A typical sequence of front propagation is displayed in Fig. 2. The front stays a while in the vicinity of the separatrix between vortices before contaminating the neighbor vortex. It is then quickly transported to the next separatrix and rolled up within the vortex. The same scenario then resumes, yielding a periodic dynamics. Meanwhile, the yet contaminated vortices continue reacting until completion of the reaction. This provides a traveling wave advancing by step with a period T in a medium of period $2L$. Its mean velocity, $V_f=2L/T$, corresponds to the effective velocity of the reaction. Measurements show that it grows with the vortex intensity U but with a decreasing efficiency (Fig. 3). The corresponding bending qualitatively agrees with that displayed in two-dimensional simulations whatever the numerical procedure [9,13]. However, it surprisingly depends here on the vortex aspect ratio l/d. Our goal is to understand its origin by carefully analyzing the way the front advances in the vortex chain.

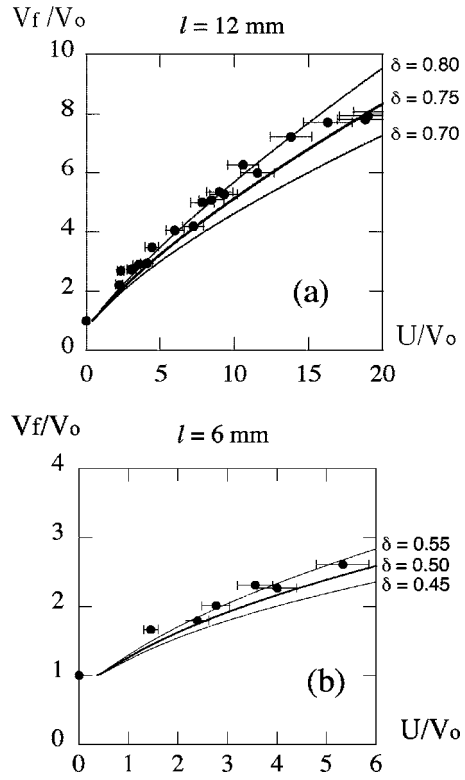

FIG. 3. Reduced effective velocity V_f/V_o as a function of reduced flow intensity U/V_o. Circles correspond to data and lines to the model predictions (5). The channel depth is $d=3$ mm and the error bars refer to the relative uncertainty on U. (a) The channel width is $l=12$ mm; $\delta=1-d/l=0.75$. (b) The channel width is $l=6$ mm; $\delta=1-d/l=0.50$.

Observations reveal disconnected front parts spread over few vortices (Fig. 2). Interestingly, in the bright colorless regions between them, reaction is completed so that concentrations are homogeneous and drive no diffusion flux. This absence of diffusion between different parts of the medium prevents front propagation to refer to a large scale reaction-diffusion wave. It thus opposes renormalization models where the effective front follows a reaction-diffusion dynamics with coefficients renormalized by the Péclet number [8,9,14].

On the other hand, observations of front dynamics in contaminated vortices reveal that fronts propagate to the vortex centers at the intrinsic velocity V_o, independently of the state of neighbor vortices. This is actually no surprise since the front being rolled up along streamlines, it advances normally to them as if the fluid was at rest: $\mathbf{U}\cdot\mathbf{n}=0$ so that $V=V_o$. This, however, indicates that front propagation involves two distinct mechanisms: the consumption of yet contaminated vortices; the contamination of additional vortices. Whereas the former sets the length of the reacting medium, the latter sets the effective front velocity.

This conclusion points to analyzing the conditions prevailing at the front head where contamination proceeds. Figure 2 shows that, after a quick advection to the next separatrix, front progression on the channel direction slows down until the next vortex is contaminated. In particular, measurements reveal that, during the crossing of the separatrix, the

front advances at about its proper velocity V_o on the channel axis, in agreement with the eïkonal dynamics since $\mathbf{U}\cdot\mathbf{n}=0$ there. However, when entering the new vortex, the front head is again advected at the flow velocity $\mathbf{U}$. It then moves on flow streamlines with a normal mainly directed along the flow: $\mathbf{n}//\mathbf{U}$. Following eïkonal dynamics, it then moves at a velocity $\mathbf{V}=\mathbf{U}+V_o\mathbf{n}$.

The modeling thus turns out determining the resulting effective velocity of a particle moving according to the above kinematics. Previous kinematic models have considered either a *single* trajectory made by vortex separatrix [13] or the *projection* of the front motion on the channel axis [9] with, for both of them, *free* boundary conditions. Both models resulted in a similar kind of relationship between V_f/V_o and U/V_o. However, motion on the vortex boundaries resulted in a velocity only half that displayed in simulations [13]. On the other hand, dynamics on the channel axis required a parameter referring to an averaged variation over the actual, but undetermined, trajectories [9]. The corresponding model was thus, in this sense, incomplete. This parameter was numerically computed on one of the trajectories found close to the vortex boundaries by numerical simulation. With its value, the model then recovered the front velocities displayed in simulations. Altogether, these studies thus support the relevance of a kinematic model for front propagation but reveal that a slight change of trajectory can dramatically modify the effective front velocity.

Following this sensitivity to trajectory, it appears essential to allow the model to determine the appropriate trajectory on which the actual front velocity has to be computed. For this, we introduce a one-parameter family of trajectories $\mathcal{F}(p)$ whose geometry is defined following those displayed by the experimental fronts. The actual trajectory is then selected as that providing the largest effective front velocity. Notice that, being the quickest of all, it will not be stopped by the encounter of a domain already burnt by another trajectory. This ensures that it will be actually achieved in practice.

Calling $\mathcal{T}$ the transit time of trajectories through a vortex, this selection turns out seeking the smallest time $\mathcal{T}(\tilde{p})$ among the trajectory family $\mathcal{F}$, the parameter $\tilde{p}$ labeling the optimal trajectory. It corresponds to a least time criterion reminiscent of Fermat's principle but applied here to a heterogeneous advective medium,

$$\frac{d\mathcal{T}}{dp}(\tilde{p})=0;\quad \frac{d^2\mathcal{T}}{dp^2}(\tilde{p})>0. \tag{1}$$

The effective front velocity then writes $V_f=L/\mathcal{T}(\tilde{p})$.

For simplicity, we consider below a square cell, the extension to rectangular cells being straightforward by an affine, area-preserving, transformation. The square size is fixed by the channel width l and *rigid* boundary conditions are applied on the channel sides (Fig. 4). The unit length is taken as $l/2$ in the following.

Following front visualization (Fig. 2), trajectories are modeled as straight paths S crossing the separatrix and connected by a circular streamline C of radius r [Fig. 4(a)]. The front head moves with velocities V_o on S and $V_o+U(r)$ on C. This provides the travel time

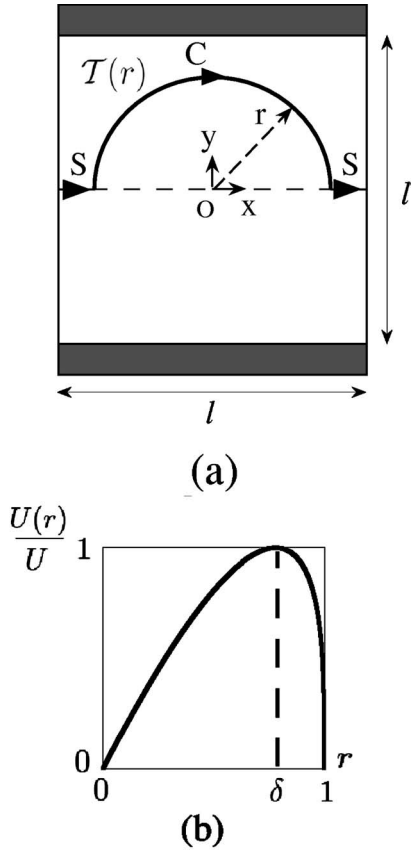

FIG. 4. Modeling of front trajectory and flow intensity. (a) Front trajectory $\mathcal{T}(r)$ made by two straight paths S enclosing a circular path C. Rigid boundary conditions apply on the dark channel sides. (b) Vortex intensity (3) involving a rigid rotation in the bulk and a boundary layer of thickness half the cell depth $d/2$, i.e., $d/l=1-\delta$ in nondimensional unit.

$$\frac{\mathcal{T}(r)}{l}=\frac{1-r}{V_o}+\frac{\pi}{2}\frac{r}{V_o+U(r)}. \tag{2}$$

To model the flow intensity $U(r)$, we stress that, in the present Hele-Shaw regime, the vertical vorticity produced at the magnet boundaries by the sudden reversion of the Laplace forces reaches a constant value beyond a boundary layer of thickness $d/2$. This means that the vortex bulk is a constant vertical vorticity domain which can be modeled by a solid rotation: $U(r)\propto r$. It ends up at a boundary layer ranging from $r=1-d/l=\delta$ to $r=1$ in nondimensional units. Asking the flow intensity to reach its maximum U at the beginning of the boundary layer yields with $dU/dr(\delta)=0$ and $U(\delta)=U$ [Fig. 4(b)],

$$U(r)=U\frac{r}{\delta}\left(\frac{1-r}{1-\delta}\right)^{(\delta^{-1}-1)}. \tag{3}$$

The optimization of the travel time among the family of trajectories can be depicted easily. The straight path $r=0$ is short but slow since the front velocity is only V_0 on it. Other paths $0<r<\delta$ are longer but faster since the front velocity raises to $V_o+U(r)$ on their circular part. All in, they are ac-

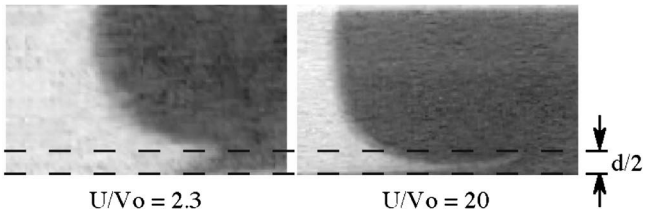

FIG. 5. Top view of front tongues showing the quickest trajectories. For slow flows, e.g., $U/V_o=2.3$, they evidence the boundary layer thickness, equal to half the cell depth $d/2$ in the present Hele–Shaw regime. The channel width l is 12 mm.

tually quicker. However, as the front velocity sharply decreases to V_o in the boundary layer, larger paths $\delta<r<1$ get slower. An optimum then takes place in between at a location labeled $\tilde{r}$.

Minimization of the travel time $\mathcal{T}(r)$ straightforwardly yields at the dominant order in U/V_o both the location $\tilde{r}$ of the fastest trajectory and the resulting effective front velocity $V_f=l/\mathcal{T}(\tilde{r})$,

$$\tilde{r}=1-(1-\delta)\left(\frac{2U}{\pi V_o}\right)^{-\delta}, \tag{4}$$

$$\frac{V_f}{V_o}=\frac{1-(1-\delta)-\left(1-\frac{2\delta}{\pi}\right)+\left(\frac{2U}{\pi V_o}\right)^{\delta}}{1-(1-\delta)\left(1-\frac{2\delta}{\pi}\right)\left(\frac{2U}{\pi V_o}\right)^{-\delta}}. \tag{5}$$

Similar relations are obtained in rectangular cells, the prefactor $\pi/2$ being replaced by 1.28 for $l=12$ mm and 1.10 for $l=6$ mm.

Evolution of the quickest trajectory with the flow intensity U/V_o is corroborated by the location of the front head near a boundary: the faster the flow, the closer the trajectory to the boundary (Fig. 5). In addition, for slow flows, i.e., $U/V_o\approx\pi/2$, relation (4) yields $\tilde{r}\approx\delta$ so that the front head stands at the end of the boundary layer, at a distance $d/2$ from the channel boundary (Fig. 5).

Figure 3 compares the model prediction (5) for the effective front velocity to the experimental data for the two channel widths: $l=12$ mm, $\delta=1-d/l=0.75$, and $l=6$ mm, $\delta=0.5$. It shows a good agreement for the two channel geometries. Interestingly, the enhancement of front velocity largely differs on both following the change of the relative size $1-\delta$ of the boundary layer [Fig. 4(b)]. This effect stresses the sensitivity of the effective front velocity to both the trajectory of the front head and the flow geometry. It weakens the meaning of a quantitative comparison with previous kinematics models [8,9,13] since they either overlooked front trajectories and vortex structures [8] or involved free boundary conditions and no boundary layer [9,13]. It nevertheless appears that the renormalization model [8] provides an asymptotic power-law trend $V_f/V_o\approx(U/V_o)^{3/4}$ which contrasts with that obtained here: $V_f/V_o\approx(U/V_o)^{\delta}$, $\delta=1-d/l$. In particular, its exponent 3/4 stands as universal whereas it appears to depend here on subscale structures, e.g., the flow boundary layer or the channel aspect ratio. Its equality with exponent δ at $l=12$ mm therefore merely stands as a coincidence that breaks down for another channel width, e.g., $l=6$ mm. Using a parameter computed on a trajectory, the kinematic model [9] determines effective front velocities that are close to those found at $l=12$ mm but far from those found at $l=6$ mm. For reasons similar to the above, the former feature here, too, stands as a coincidence.

In conclusion, we have performed experiments on front propagation in a vortex chain. Fronts alternate quick advection inside a vortex and slow crossing of their separatrix. Their mean velocity along the chain shows a dependence on both the width and depth of vortices. This indicates a sensitivity of front dynamics to the flow structure which calls for modeling the front trajectory inside a vortex. We achieved this by considering a one-parameter family of trajectory and a vortex flow involving rigid rotation and a boundary layer. The actual trajectory is selected from a least time criterion as the quickest one. It enabled us to finely recover the mean front velocity and its variation with the vortex aspect ratio. Interestingly, this agreement is obtained for simple models of flow and trajectories. This gives confidence in the efficiency of the least time criterion to successfully select front trajectories and front velocities in more complex configurations.

[1] R. J. Field and M. Burger, *Oscillations and Traveling Waves in Chemical Systems* (Wiley, New York, 1985).
[2] F. A. Williams, *Combustion Theory* (Benjamin-Cummings, New York, 1985).
[3] J. D. Murray, *Mathematical Biology* (Springer-Verlag, Berlin/Heidelberg, 1993).
[4] G. Searby and J. Quinard, Combust. Flame **82**, 298 (1990).
[5] M. Leconte, J. Martin, N. Rakotomalala, and D. Salin, Phys. Rev. Lett. **90**, 128302 (2003).
[6] M. S. Paoletti and T. H. Solomon, Europhys. Lett. **69**, 819 (2005); Phys. Rev. E **72**, 046204 (2005).
[7] F. Harambat, Ph.D. thesis, Université de Provence, 2005 (unpublished).
[8] M. Abel, A. Celani, D. Vergni, and A. Vulpiani, Phys. Rev. E **64**, 046307 (2001).
[9] M. Abel, M. Cencini, D. Vergni, and A. Vulpiani, Chaos **12**, 481 (2002).
[10] I. R. Epstein and K. Kustin, J. Phys. Chem. **89**, 2275 (1985).
[11] H. Willaime, O. Cardoso, and P. Tabeling, Phys. Rev. E **48**, 288 (1993).
[12] B. F. Edwards, Phys. Rev. Lett. **89**, 104501 (2002).
[13] N. Vladimirova, P. Constantin, A. Kiselev, O. Ruchayskiy, and L. Ryzhik, Combust. Theory Modell. **7**, 485 (2003).
[14] B. Audoly, H. Berestycki, and Y. Pomeau, C. R. Acad. Sci., Ser. IIb: Mec., Phys., Chim., Astron. **328**, 255 (2000).